


PAPER

Fast switch from extensional exhumation to thrusting of the Ronda Peridotites (South Spain)

Gianluca Frasca^{1,2}  | Frédéric Gueydan² | Marc Poujol¹ | Jean-Pierre Brun¹ | Fleurice Parat² | Patrick Monié² | Alexandre Pichat² | Sophie Mazier¹¹Géosciences Rennes, UMR 6118 CNRS/INSU, OSUR, Université Rennes 1, Rennes Cedex, France²Géosciences Montpellier, Université Montpellier, UMR 5243 CNRS/INSU, Montpellier Cedex, France**Correspondence**Gianluca Frasca, Géosciences Rennes, UMR 6118 CNRS/INSU, OSUR, Université Rennes 1, Rennes Cedex 35042, France.
Email: gianluca.frasca@univ-rennes1.fr**Funding information**

European Union FP7 Marie Curie ITN "TOPOMOD", Grant/Award Number: 264517;

Abstract

The Alboran Domain, situated at the western end of the Mediterranean subduction system, is characterized by the Ronda Peridotites, one of the world's largest exposures of sub-continental mantle. Using U–Pb (LA-ICP-MS) and Ar–Ar dating, we precisely dated two tectonic events associated with the Tertiary exhumation of the Ronda Peridotites. First, shearing along the Crust–Mantle Extensional Shear Zone caused, at ca. 22.5 Ma, mantle exhumation, local partial melting in the deep crust and coeval cooling in the upper crust. Second, the Ronda Peridotites Thrust triggered the final emplacement of the peridotites onto the continental crust at c. 21 Ma, as testified by granitic intrusions in the thrust hangingwall. The tectonic evolution of the western Alboran Domain is therefore characterized by a fast switch from continental lithospheric extension in a backarc setting, with sub-continental mantle exhumation, to a rift inversion by thrusting driven by shortening of the upper plate.

1 | INTRODUCTION

The Mediterranean is characterized by the coexistence of backarc basins and arcuate subduction zones caused by slab rollback (e.g. Calabria, Hellenic trench; Wortel & Spakman, 2000). The Gibraltar arc (Betics in Spain and Rif in Morocco) is marked by the exhumation of large bodies of sub-continental mantle, the Ronda Peridotites, whose role in the geodynamics of the western Mediterranean is still debated (Garrido et al., 2011; Van Hinsbergen et al., 2014). The polycyclic history of the Ronda lithospheric section makes it difficult to unequivocally link slab rollback evolution and sub-continental mantle exhumation, as proposed for the central Mediterranean backarc system (Acosta-Vigil et al., 2016; Bache et al., 2010; Sánchez-Rodríguez & Gebauer, 2000).

The Ronda Peridotites consist of a tectonic sliver within the Alboran crust, bounded by two major tectonic contacts. A Crust–Mantle Extensional Shear Zone at the top of the Ronda Peridotites accommodated extreme continental lithospheric thinning (CMESZ, red in Figure 1; Afiri et al., 2011; Argles et al., 1999; Frasca et al., 2016; Précigout et al., 2013). The crustal rocks overlying the peridotites

comprise a strongly attenuated crustal section (Balanyá et al., 1997). The metamorphic grade decreases continuously from granulite facies to un-metamorphosed rocks in the 4-km-thick crustal sequence above the Ronda Peridotites (Argles et al., 1999; Balanyá et al., 1997; Barich et al., 2014). Furthermore, shearing in the granulites was coeval and consistent with garnet–spinel mylonitization at the top of the mantle (Frasca et al., 2016; Précigout et al., 2013). However, the age of this continental lithospheric thinning is still debated. In the granulites, garnet rims and part of the matrix crystallized during the Tertiary (Massonne, 2014; Platt, Whitehouse, et al., 2003; Whitehouse & Platt, 2003). A much older partial melting event has been proposed from c. 1.4–1.2 GPa to 0.6–0.5 GPa at around 800°C for part of the Ronda crustal section in Hercynian times (Barich et al., 2014; Ruiz Cruz & Sanz de Galdeano, 2014). Furthermore, Jurassic ages have been obtained in pyroxenite layers within the peridotites (Sánchez-Rodríguez and Gebauer, 2000).

The Ronda Peridotites Thrust (RPT, blue in Figure 1; Frasca et al., 2015; Lundeen, 1978; Mazzoli and Martín-Algarra, 2011; Vitale et al., 2014) marks the second tectonic contact of the peridotites. The rocks below the Ronda Peridotites are highly diverse, with

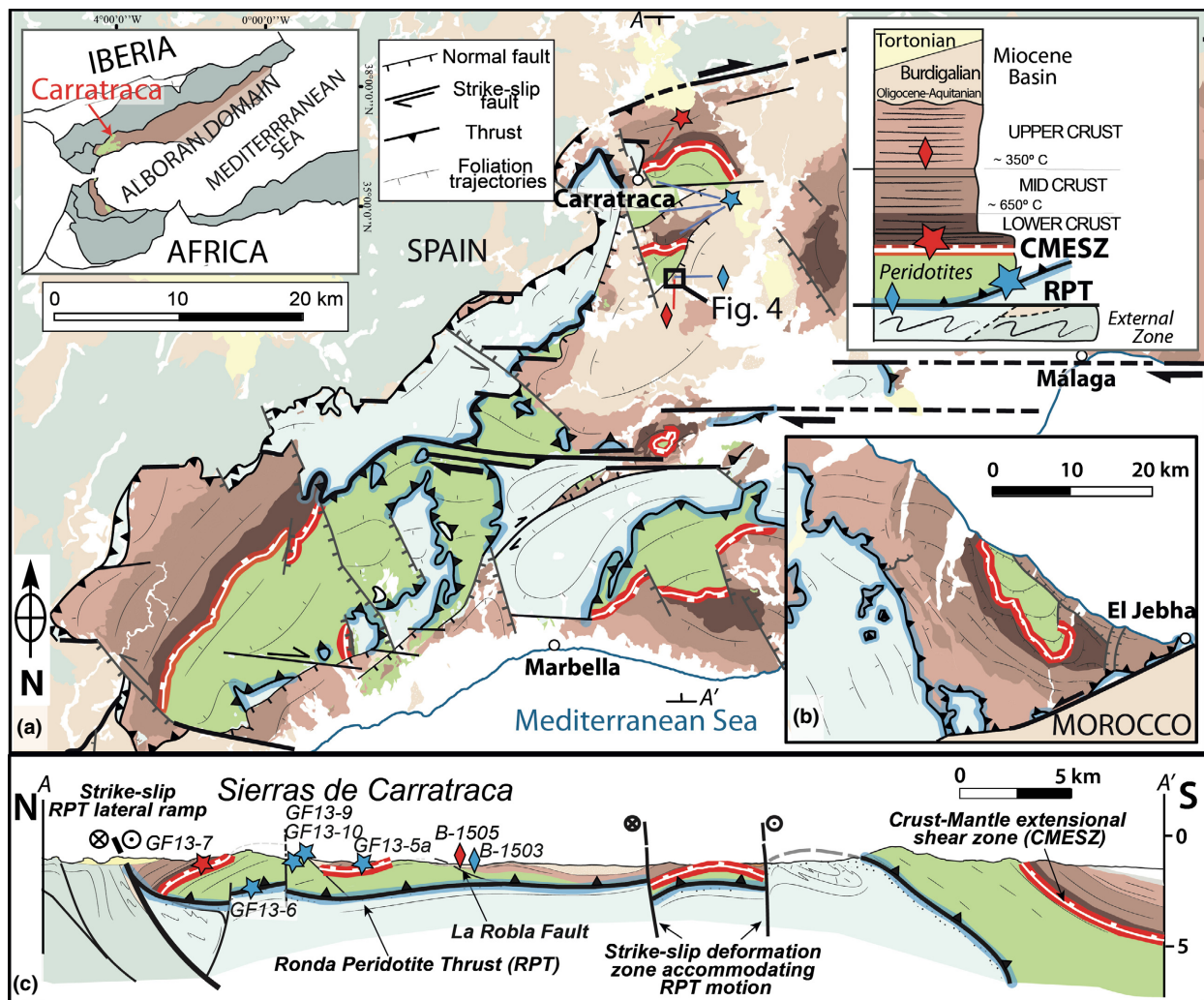


FIGURE 1 (a) Tectonic map of the Ronda Peridotites massifs (from Frasca et al., 2015), showing the sampling locations in the Carratraca area. A and A' are the endpoints of the cross-section line shown in (c). Inset: position of the Alboran Domain between the Nubia and Iberia plates, showing the locations of sub-continental mantle and of the studied area. RPT, Ronda Peridotites Thrust (blue); CMESZ, Crust-Mantle Extensional Shear Zone (red). (b) Tectonic map of the Beni Bousera peridotites massif (modified after Afri et al., 2011). Colours are illustrated in the generalized vertical section at the top right of (a). (c) Simplified N-S regional cross-section. Note the strike-slip deformation zones that laterally accommodate the RPT motion. Stars and diamonds indicate the positions of the samples collected for U-Pb and Ar-Ar analyses respectively (blue: rift-related sample; red: thrust-related sample) [Colour figure can be viewed at wileyonlinelibrary.com]

variable degrees of metamorphism from low-grade limestones to strongly mylonitized marbles (see summary in Frasca et al. (2015)). Migmatites in the footwall and granitic dikes intruding the mantle and the crustal hangingwall yield a cluster of crystallization ages between 23 and 19 Ma (Esteban et al., 2011; Monié et al., 1994; Rossetti et al., 2010; Sánchez-Rodríguez & Gebauer, 2000; Sosson et al., 1998). A thermal overprint on Hercynian migmatites in the thrust footwall during the Tertiary has been also reported (Acosta-Vigil et al., 2014). A major shortening event during the Miocene therefore triggered the final crustal emplacement of the Ronda Peridotites (Précigout et al., 2013; Tubía et al., 1997).

These first-order geological features have yielded a diversity of tectonic models for the exhumation of the Ronda Peridotites from mantle depths to the surface. The three main models are: (1) exhumation during the Hercynian orogeny (collision/collapse) with

only passive reworking during the Alpine orogeny (Massonne, 2014; Ruiz Cruz & Sanz de Galdeano, 2014); (2) exhumation during the Tethysian rifting, followed by the subduction of the Tethyan passive margin (and its lithospheric mantle) during the complex Alpine phase (Tubía et al., 1997; Van der Wal & Vissers, 1993) and (3) Oligo-Miocene exhumation during westward Alboran slab roll-back, followed by rift inversion during the lower Miocene (Garrido et al., 2011; Gueydan et al., 2015; Marchesi et al., 2012; Précigout et al., 2013).

To discriminate between these models, we provide new ages (U-Pb LA-ICP-MS and Ar-Ar) obtained on syn-deformational structures related to both thinning and thrusting. The ages clearly separate two successive crustal-melting events structurally associated with the Ronda Peridotites. We compare the new ages with the available datasets in the region and discuss their geodynamic implications.

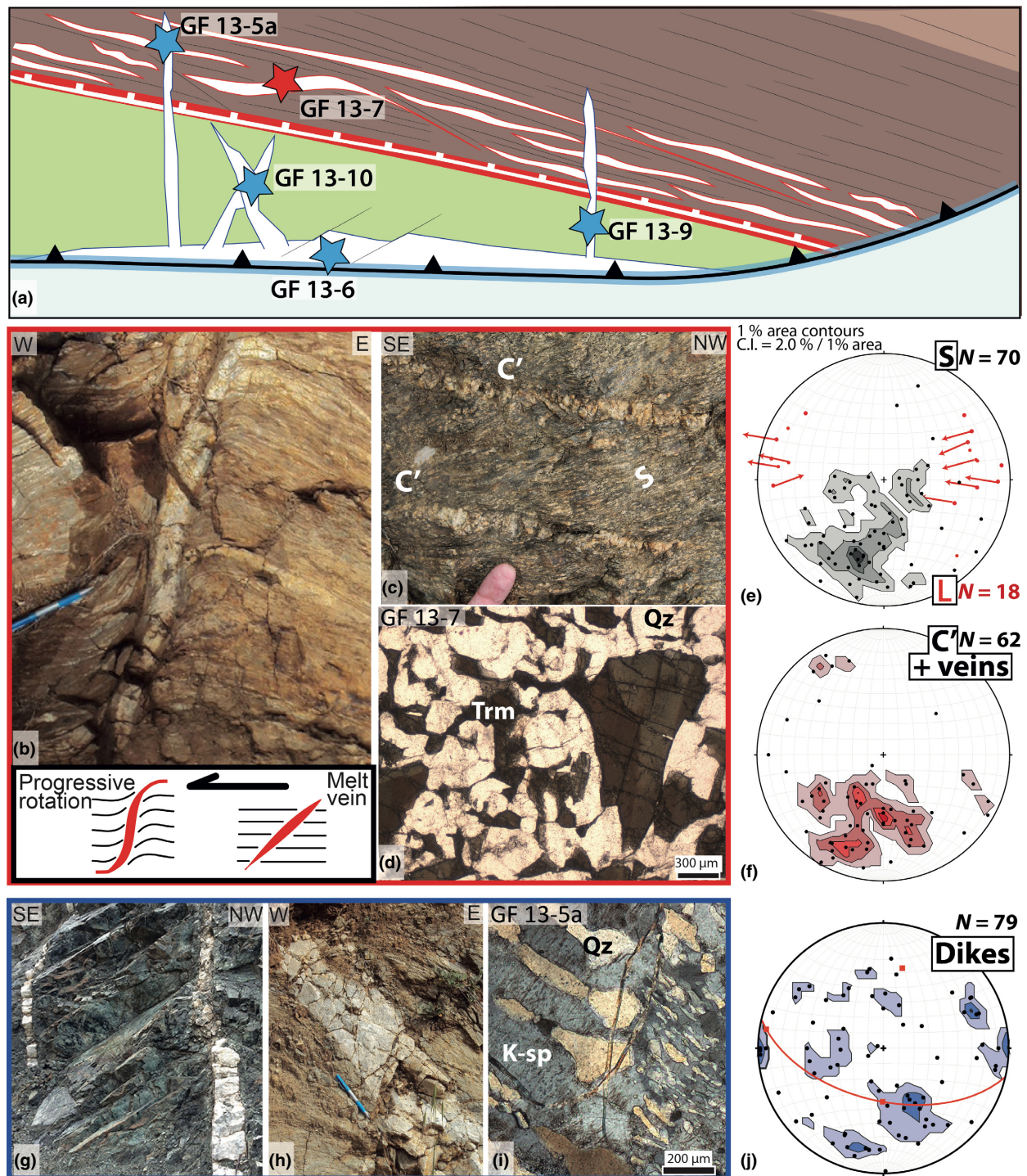


FIGURE 2 (a) Schematic relationships (not to scale) between peridotites, overlying rocks and metamorphic sole, with structural positions of the samples selected for U–Pb studies. (b) Melt vein rotated during progressive top-to-the-west shearing (evolution shown in the diagram). (c) Syn-kinematic leucocratic vein within C'-type shear band in the deep crust. (d) Graphic texture between zoned tourmaline and quartz (GF13-7); plane-polarized light. (e) Stereoplot of foliations in the lower crust, with stretching lineations along the CMESZ and associated sense of shear (lower hemisphere; Schmidt net); data from the Sierras de Carratraca. (f) Stereoplot of the melt syn-kinematic veins in the lower crust (Carratraca area). (g) Undeformed granite intrusion in the peridotites. (h) Dike cross-cutting the regional foliation in the granulite of the lower crust. (i) Granophyric textures of different sizes testifying to the different phases of crystallization of K-feldspar–quartz intergrowths in a melt (GF13-5a); crossed-polarized light. (j) Stereoplot of the dikes and sills cutting through the peridotites and dikes cutting the regional foliation in the lower crust (Carratraca area). GPS locations of the sampled outcrops can be found in Table S9 [Colour figure can be viewed at wileyonlinelibrary.com]

TABLE 1 Major, trace element and isotopic compositions of the melt products sampled in the Ronda Peridotites and their crustal envelope. ASI = $\text{Al}_2\text{O}_3/(\text{Na}_2\text{O}-1.67\text{P}_2\text{O}_5+\text{K}_2\text{O}+\text{CaO})$, molar; A/NK = $\text{Al}_2\text{O}_3/(\text{Na}_2\text{O}+\text{K}_2\text{O})$, molar; A/2CNK = $\text{Al}_2\text{O}_3/(\text{CaO}+\text{Na}_2\text{O}+\text{K}_2\text{O})$, molar

Sample	GF13-7	GF13-6	GF13-5A
SiO ₂ (wt.%)	73.66	75.99	83.05
TiO ₂	0.14	0.06	0.09
Al ₂ O ₃	14.00	13.24	8.19
FeOt	1.81	0.68	0.72
MnO	0.02	0.01	0.01
MgO	0.36	0.48	0.18
CaO	1.33	1.95	0.61
Na ₂ O	3.61	4.80	1.51
K ₂ O	2.64	0.74	4.31
P ₂ O ₅	0.14	0.05	0.03
LOI	1.57	0.87	0.93
Total	99.28	98.87	99.63
ASI	1.27	1.09	1.00
A/NK	1.59	1.52	1.15
A/2CNK	1.03	0.84	0.87
Be (ppm)	<1	5	2
Sc	7	6	<1
V	16	5	8
Cr	120	190	150
Co	4	3	2
Ni	<20	<20	<20
Rb	96	20	144
Sr	405	204	82
Y	24	13	3
Zr	66	42	41
Nb	11	7	4
Sn	8	5	2
Cs	1.4	<0.5	2
Ba	407	878	271
La	11.1	13.6	20.2
Ce	22.8	27.1	42.6
Pr	2.62	3.03	4.97
Nd	9.7	10.2	18.2
Sm	2.8	2.9	4.1
Eu	1.03	0.85	0.78
Gd	2.8	2.3	2
Tb	0.6	0.4	0.2
Dy	4.2	2.6	0.8
Ho	0.9	0.5	0.1
Er	2.6	1.3	0.3
Tm	0.48	0.21	0.05
Yb	3.9	1.3	0.2
Lu	0.62	0.17	0.04

(Continues)

TABLE 1 (Continued)

Sample	GF13-7	GF13-6	GF13-5A
Hf	1.9	1.8	1.5
Ta	2.1	1.8	0.3
W	13	<1	<1
Tl	0.3	<0.1	0.5
Pb	23	12	32
Bi	<0.4	<0.4	<0.4
Th	3.4	5.8	12.2
U	4.4	6.6	13.3
⁸⁷ Sr/ ⁸⁶ Sr (standard)	0.718605	0.720831	0.719869
±2σ	0.000013	0.000012	0.000012
¹⁴³ Nd/ ¹⁴⁴ Nd (standard)	0.512026	0.512068	0.512140
±2σ	0.000005	0.000004	0.000006
¹⁴⁷ Sm/ ¹⁴⁴ Nd	0.15528	0.14569	0.12805
εNd(t)	-11.26	-10.99	-9.54

2 | TWO SUCCESSIVE CRUSTAL-MELTING EVENTS

2.1 | Structural setting

Two types of intrusion were sampled from the Ronda Peridotites and their crustal envelope (for positions of the samples, see the regional map and the N–S cross-section in Figure 1a,c and a more precise structural location on the schema in Figure 2a): (1) a syn-deformational melt vein in the deepest part of the crust overlying the peridotites, in the Crust–Mantle Extensional Shear Zone (GF13-7; Figure 2b–d) and (2) four leucocratic dikes cross-cutting the main foliations either of the Ronda Peridotites or of the overlying deep crust (GF13-6, GF13-9, GF13-10 and GF13-5a) (Figure 2g–i).

The syn-deformational intrusions (e.g. GF 13-7) are structurally associated with a top-to-the-W shearing along the Crust–Mantle Extensional Shear Zone (Frasca et al., 2016; Précigout et al., 2013). Syn-deformational intrusions are located either in veins that rotated during shearing (Figure 2b) or along C'-type shear bands in the high-temperature granulitic foliation (Figure 2c). C'-type shear bands are slightly oblique to the regional high-temperature foliation, whereas veins cut the foliation at higher angles (see stereoplots in Figure 2e,f).

In contrast, the undeformed dikes intruding the Ronda Peridotites and the crustal envelope (GF 13-5a, GF13-6, GF 13-9 and GF 13-10) crosscut the regional foliation (Figure 2g,h) and show a random distribution in the stereographic projection (Figure 2j). These dikes are therefore unrelated to the high-temperature foliations (stereoplot in Figure 2j) and their source is structurally identified below the Ronda Peridotites (Figure 2a). This second type of intrusion was thus emplaced during the motion of the Ronda Peridotite Thrust.

2.2 | Petrography and geochemistry

A magmatic origin for the syn-deformational and undeformed sampled intrusions is clearly indicated by interlocking, graphic and

granophytic textures (Figure 2d,i; see also Cuevas et al., (2006, and Barich et al., 2014). U–Pb LA-ICP-MS dating and Nd and Sr isotope analyses were performed at Géosciences Rennes following the procedures described in Ballouard et al. (2015) (see Tables S1 and S2 for details and operating conditions of the LA-ICP-MS measurements).

The isotopic signature of the dikes is similar to those of other Alboran Domain granites (Rossetti et al., 2013) and references therein). The high $^{87}\text{Sr}/^{86}\text{Sr}$ (0.715037, GF13-9 and 0.718605, GF13-7) and the low $^{143}\text{Nd}/^{144}\text{Nd}$ (0.512020, GF13-9 and 0.512026, GF13-7) values indicate a predominantly crustal origin for both types of dikes, compatible with dehydration melting of a metasedimentary source (Table 1). However, the different structural contexts (Figure 2a) and the large differences in their rare-earth element geochemistry (REE, Figure 3a) suggest different timings and different sources for the melt, as supported by their respective TDM (i.e. Time Depleted Mantle model age) values of 1,270 and 2,600 Ma (Tables S3 and S5).

2.3 | In situ melting in the lower crust above the peridotites at ca. 22.5 Ma

The syn-deformational intrusion in a shear zone located inside the granulites (GF13-7) is peraluminous, mainly composed of K-feldspar, quartz and plagioclase, with accessory tourmaline, and presents a concave REE pattern (Figure 3a). This enrichment in heavy REE

suggests that garnet was consumed in the melting reaction (Figure 3a and Table 1).

Cathodoluminescence (CL) images of the zircon grains (Figure 3b insets) show distinct cores and rims for some of them, although, when euhedral, the grains are fairly homogeneous. The cores yield dates ranging from Neoproterozoic to Cretaceous (Table S3) in good agreement with the TDM value for this sample (Table S3). The rims and the homogeneous grains give consistent Miocene dates. In a Tera-Wasserburg diagram, these analyses plot in a concordant to sub-concordant position (Figure 3b). The concordant data yield a concordia age of 22.52 ± 0.16 Ma (MSWD = 1.4, $n = 16$), consistent with a mean $^{206}\text{Pb}/^{238}\text{U}$ age of 22.52 ± 0.18 (MSWD = 1.6, $n = 20$).

2.4 | Undeformed dikes: melt extraction from the metamorphic sole below the Ronda Peridotites at c. 20 Ma

Undeformed dikes intruding the peridotites and the overlying crustal rocks (GF13-6, GF13-5a) have a chondrite-normalized REE pattern enriched in light REE and depleted in heavy REE compared with the extensional-related sample (GF 13-7), suggesting a lower degree of partial melting and different sources (Figure 3a). Our samples GF13-6 and GF13-5a present REE patterns similar to those of Rossetti et al. (2013) from the Rif (Figure 3a). These rocks also contain slightly more plagioclase and biotite than sample GF13-7, and often titanite.

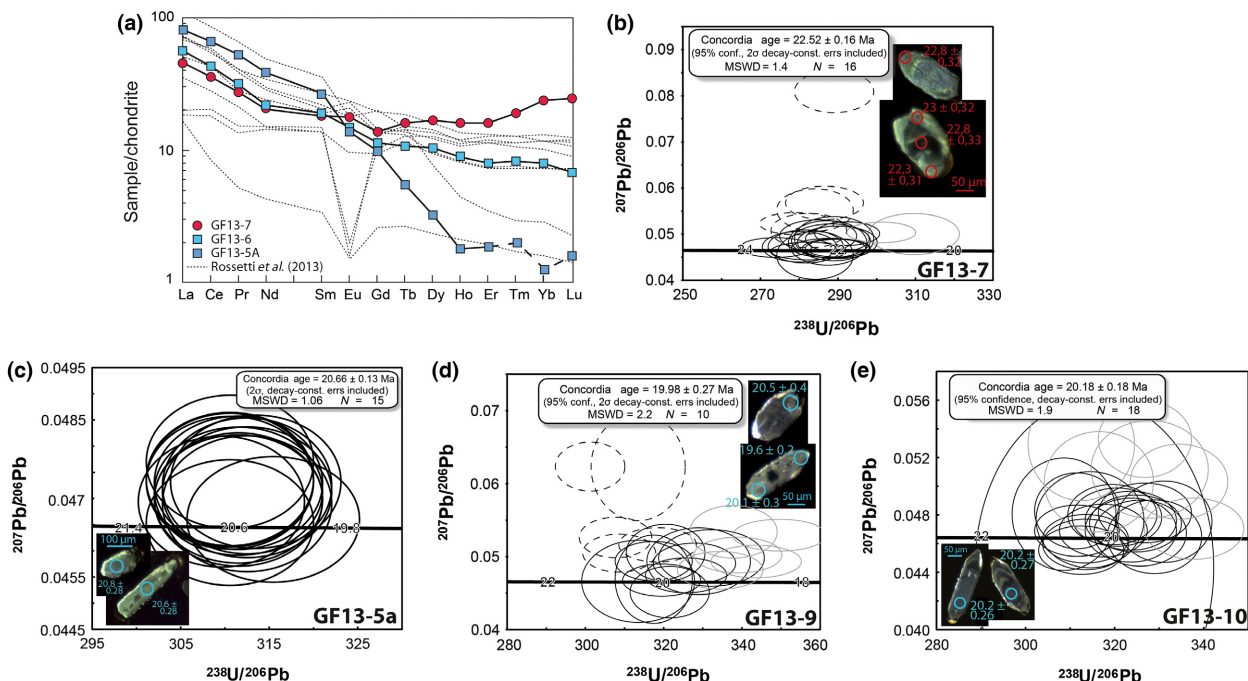


FIGURE 3 (a) Different chondrite-normalized patterns for the collected samples and those of Rossetti et al. (2013). (b–e) Concordia diagrams for the time interval between c. 25 and 18 Ma, showing LA-ICP-MS U–Pb zircon analyses for samples GF13-7, GF 13-5a, GF13-9 and GF13-10. Error ellipses are at 2σ . Plain back ellipses: analyses used for Concordia age calculations; dashed ellipses: data with common Pb; light grey ellipses: data with slight Pb loss. Insets show CL pictures of some of the grains dated in this study together with the obtained $^{206}\text{Pb}/^{238}\text{U}$ dates. Data tables are available in supporting information [Colour figure can be viewed at wileyonlinelibrary.com]

The dike from which GF13-5a was sampled crosscuts the granulite foliation. Of the zircon grains studied from this sample, three inherited cores give a Palaeozoic date of 337.2 ± 0.13 Ma (MSWD = 0.21) (Table S4), whereas the remaining 15 data points are concordant (Figure 3c) and yield a concordia age of 20.66 ± 0.13 Ma (MSWD = 1.06; $n = 15$) with a mean $^{206}\text{Pb}/^{238}\text{U}$ age of 20.65 ± 0.13 Ma (MSWD = 0.17; $n = 15$) (Table S4). The inherited components are far less abundant than in the extensional-related sample GF13-7 and indicate a different origin, suggesting two distinct partial melting events.

Samples GF13-9 and GF13-10 consistently show inherited components similar to sample GF13-5a, suggesting a different origin from sample GF13-7. In sample GF13-9, analyses plot in a concordant to discordant position depending on the degree of Pb loss and/or the presence of common Pb (Figure 3d). A group of 10 concordant analyses yield a concordia age of 19.98 ± 0.27 Ma

(MSWD = 2.2; $n = 10$) and a mean $^{206}\text{Pb}/^{238}\text{U}$ age of 20.14 ± 0.25 Ma (MSWD=2.4, $n = 14$) (Table S5).

For sample GF13-10, zircon CL images show rare grains with distinct cores and rims. Only three cores were dated and give Palaeozoic dates. The remaining data points give Miocene dates. The most concordant data (Figure 3e) define a concordia age of 20.18 ± 0.18 Ma (MSWD = 1.9; $n = 18$), in agreement with the mean $^{206}\text{Pb}/^{238}\text{U}$ age of 20.08 ± 0.20 Ma (MSWD = 2.6; $n = 23$) (Table S6).

3 | AGES OF EXTENSION AND THRUSTING IN SEMI-BRITTLE STRUCTURES

Lower-crustal melting during thinning is coeval with upper-crustal shearing accommodated by C'-type extensional shear planes (Figure 4a,b and structural details in Frasca et al., 2016). $^{40}\text{Ar}/^{39}\text{Ar}$

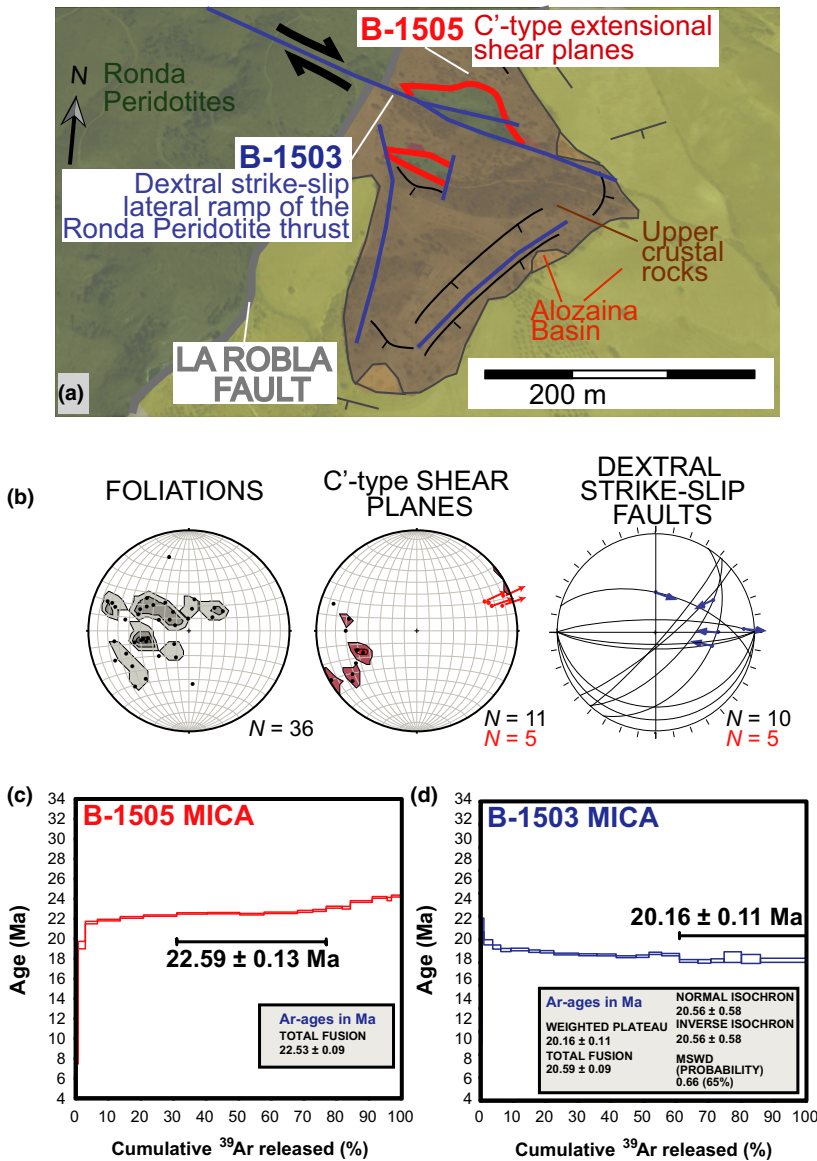


FIGURE 4 (a) 3D visualization of the southeastern termination of the Carratraca massif, with the geological contours superposed on the topography from GoogleEarth©. Grey and red: rift-related La Robla normal fault and El Chenil Low Angle Normal Fault (LANF). Blue: rift-inversion-related compressional and strike-slip faults (modified after Frasca et al., 2016). For location and details of colours see Figure 1. GPS locations of the sampled outcrops can be found in Table S9. (b) Stereoplots of data collected in the area of (a) (lower hemisphere; Schmidt net): foliations in the upper crustal rocks, stretching lineations and associated C'-type shear bands with the arrow indicating the sense of shear (OSXStereonet: version 9.2.0. <http://www.ux.uis.no/~nestor/work/programs.html>); and rift-inversion-related fault surfaces (great circles) with slip vectors (blue arrows) (FSA software by Célérier <http://www.bcelierier.univ-montp2.fr/bc.home.e.html>: version 35.2). (c,d) $^{40}\text{Ar}/^{39}\text{Ar}$ age spectra for white mica extracted from samples B-1503 (rift-related structure) and B-1505 (thrust-related structure; see method and analytical data in Tables S1 and S7 in supporting information) [Colour figure can be viewed at wileyonlinelibrary.com]

step-heating analysis of the white mica along these C'-type shear planes (Sample B-1505, Figure 4c) yields a discordant age spectrum due to the mixing of two generations of mica, with a young component dated around 20 Ma and an older one of 24 Ma or older. Therefore, the intermediate segment at 22.59 ± 0.13 Ma is meaningless (Figure 4c). The rift-related structures are then crosscut by thrust-related structures (thrusts and dextral strike-slip faults, see details in Frasca et al., 2015). $^{40}\text{Ar}/^{39}\text{Ar}$ step-heating analysis of the white mica extracted from the matrix of the tectonic breccia (Sample B-1503, Figure 4d) along one of the dextral strike-slip lateral ramps of the Ronda Peridotites Thrust (see stereoplot in Figure 4b) gives a plateau age of 20.16 ± 0.11 Ma at the end of degassing, after the release of an excess argon component for 60% of ^{39}Ar (see the age spectrum in Figure 4d, complete isotopic results in Table S7 and method details in Table S1). Note that the two generations of mica in sample B1505 (rift-related structure, Figure 4c) may reflect these two stages of deformation, with the old ages at c. 24 Ma related to rifting and the young ages at c. 20 Ma related to thrusting.

4 | DISCUSSION AND CONCLUSION

The coupling of geochronological and geochemical data with the regional structures allows us to identify and date two distinct tectonic events during the Lower Miocene, related to mantle exhumation and its final thrust emplacement: (1) lithospheric thinning in a backarc setting leading to in-situ melting at c. 22.5 Ma, coherent with C'-type extensional shear bands in the mid/upper crust (Ar–Ar ages) and (2) rift inversion marked by a hot thrusting of the Ronda Peridotites and the overlying crustal envelope onto the continental crust, dated at c. 20 Ma by undeformed dikes cross-cutting the former HT foliation (in both the peridotites and the overlying high-grade crustal rocks) and by brittle thrust-related faults. The differences in geochemistry, age and structural setting unequivocally separate these two different crustal-melting events (Figure 5).

The new age of c. 22.5 Ma for the rift-related structures is compatible with previous geochronological data attesting to Oligo-Miocene rifting in the Alboran Domain: U–Pb ages of 22.0 ± 0.3 Ma and 22.7 ± 0.3 Ma, obtained on zircon rims from granulites (Platt et al., 2003) in Ronda and Beni Bousera (Moroccan equivalent of the Ronda peridotites); LA-ICP-MS ages of 21.3 ± 0.3 Ma obtained on syn-foliation monazites within the granulites, and an $^{40}\text{Ar}/^{39}\text{Ar}$ biotite age of 22.5 ± 0.5 Ma from granulites overlying the Beni Bousera Peridotites (Gueydan et al., 2015; Michard et al., 2006).

The new ages of ca. 20 Ma for the dikes intruding the thinned lithosphere (GF13-5a, GF13-9 and GF13-10) are relatively younger than suggested by some previous U–Pb data (Figure 5). The older ages of dikes intruding the peridotites (21.5 ± 3.8 and 22.6 ± 1.8 Ma; Esteban et al., 2011) suggest a possible onset of thrusting at 22–21 Ma, although the large

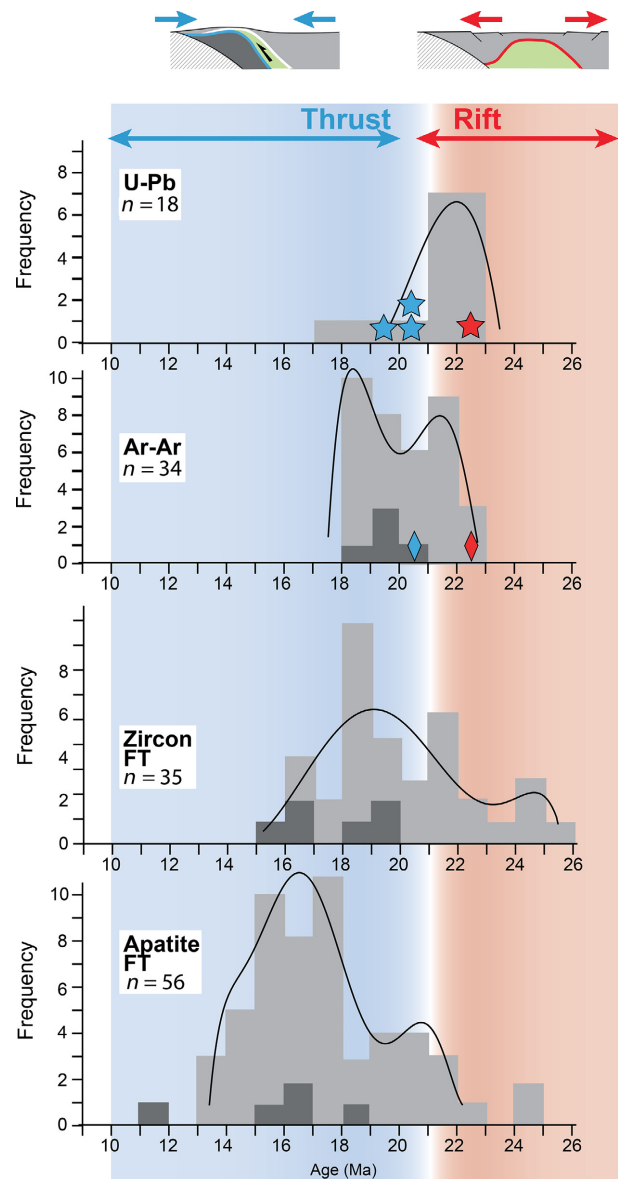


FIGURE 5 Frequency distribution of the ages available for the western Betics, Rif, ODP Leg 161 and ages obtained in our study (symbols as in Figure 1). The black line is the best approximation of the trend of the data (polynomial degree 7), excluding the extremity values. From top to bottom: (i) U–Pb on zircons (Esteban et al., 2007, 2011; Platt & Whitehouse, 1999; Platt, Whitehouse, et al., 2003; Sánchez-Rodríguez & Gebauer, 2000); (ii) $^{40}\text{Ar}/^{39}\text{Ar}$ on mica (Chalouan et al., 2008; Frasca et al., 2016; Kelley & Platt, 1999; Monié et al., 1994; Platt, Argles, et al., 2003; Rossetti et al., 2010; Sosson et al., 1998) and (iii) fission tracks on zircon (Azdimousa et al., 2014; Esteban et al., 2004, 2005, 2007; Platt, Argles, et al., 2003) and apatite (Azdimousa et al., 2014; Esteban et al., 2004, 2005; Hurford et al., 1999; Platt, Argles, et al., 2003; Sosson et al., 1998). Pale and dark grey colours in the histograms correspond to samples above and below the RPT respectively. The bimodal distributions of Ar–Ar, ZFT and AFT ages are well correlated with the two Lower Miocene tectonic events (syn-rift in red and rift inversion in blue; see sketches on top) [Colour figure can be viewed at wileyonlinelibrary.com]

errors affecting the concordia ages and the limited number of analysed zircon grains do not permit precise dating. Zircon ages of 21.79 ± 0.6 (younger intersection on the concordia diagram) and 22.3 ± 0.2 Ma (weighted $^{206}\text{Pb}/^{238}\text{U}$ mean age), reported from dikes in the thinned continental crust above the peridotites, have been interpreted as a metamorphic imprint on Hercynian partial melting products or as thrust-related intrusion (Rossetti et al., 2010; Sánchez-Navas et al., 2014). Ar–Ar data on biotites from undeformed granites (Monié et al., 1994; Sossion et al., 1998) and the Ar–Ar plateau age on white mica from thrust-related structures presented in this study support thrusting at 21–20 Ma. Finally, a major change in sedimentation in both the external and the internal domains at around 20 Ma is interpreted as a marker of the onset of thrusting in the Western Betics (see Serrano et al., 2007, and review in Frasca et al. 2015).

The compilation of available geochronological data for the Western Alboran domain (western Betics and Rif) shows a bimodal distribution of Ar–Ar ages on mica, zircon fission track (ZFT) and apatite fission track (AFT) ages, suggesting two distinct cooling events related to the two crustal-melting events reported here (Figure 5, Table S8). A first cooling event occurred between 25 and 22–20 Ma and may mark the late stage of continental rifting (Figure 5, see discussion in Frasca et al., 2016). However, the majority of ages using medium- to low-temperature thermochronometers are younger than 20 Ma (Figure 5). The absence of older ages in the thrust footwall (see ages in dark grey in Figure 5; Esteban et al., 2013; Monié et al., 1994) supports a reset of these low-temperature thermochronometers during heating at ca. 21 Ma, as a consequence of the hot emplacement of the peridotites nappe on a colder crustal unit (Figure 5), followed by a general fast cooling. The characteristic time for cooling (t_c) is controlled by the thickness of the thrust sheet (the Ronda Peridotites and their crustal envelope) and its thermal diffusivity, $t_c = d^2/K$, where $K = 10^{-6} \text{ m}^2/\text{s}$ (Turcotte & Schubert, 1982). Taking 10 km as an average thrust sheet thickness yields a characteristic time of 3.17 Ma for the conductive cooling of the thrust sheet, explaining the regional fast cooling starting at c. 21 Ma.

At the regional scale, the tectonic history of the Ronda Peridotites is the result, during slab rollback, of a fast switch at c. 21 Ma from exhumation driven by back-arc extension (i.e. rifting) to a thrust emplacement of the overriding plate onto the Iberian margin. This sequence of events, from rifting between 30 and 21 Ma to thrusting at c. 21 Ma, is consistent with the geodynamic model of Duggen et al. (2004), based on geochemical tracers: subduction processes (marked by the Malaga tholeiite dikes) followed by nappe emplacement (marked by crustal melting). A remaining key issue is to identify the exact location of the rift inversion, either to the north of the Algerian margin or close to the present-day position of the Gibraltar arc. These two hypotheses would imply either a large (e.g. Hidas et al., 2013) or a limited (e.g. Frasca et al., 2015) amount of rollback since 20 Ma respectively.

ACKNOWLEDGEMENTS

This work was funded by the European Union FP7 Marie Curie ITN “TOPOMOD”, contract 264517. We thank A. Delplanque and P. Frasca for help in drawing Figure 5 and to Bernard Célérier for useful discussions. Very constructive comments made by David Chew, an anonymous reviewer, the Associate Editor and Editor helped to improve the manuscript.

REFERENCES

- Acosta-Vigil, A., Rubatto, D., Bartoli, O., Cesare, B., Meli, S., Pedrera, A., Azor, A. and Tajcmanova, L. (2014). Age of anatexis in the crustal footwall of the Ronda Peridotites. *S. Spain. Lithos*, 210, 147–167.
- Acosta-Vigil, A., Barich, A., Bartoli, O., Garrido, C., Cesare, B., Remusat, L., Poli, S., & Raepsaet, C. (2016). The composition of nanogranitoids in migmatites overlying the Ronda peridotites (Betic Cordillera, S Spain): The anatectic history of a polymetamorphic basement. *Contributions to Mineralogy and Petrology*, 171(24), 1–31.
- Afiri, A., Gueydan, F., Pitra, P., Essai, A., & Précigout, J. (2011). Oligo-miocene exhumation of the Beni-Boussera peridotite through a lithosphere-scale extensional shear zone. *Geodinamica Acta*, 24(1), 49–60.
- Argles, T., Platt, J., & Waters, D. (1999). Attenuation and excision of a crustal section during extensional exhumation: the Carratraca massif, Betic Cordillera, southern Spain. *Journal of the Geological Society*, 156 (1), 149–162.
- Azdimousa, A., Bourgeois, J., Poupeau, G., Vázquez, M., Asebriy, L., & Labrin, E. (2014). Fission track thermochronology of the Beni Boussera peridotite massif (Internal Rif, Morocco) and the exhumation of ultramafic rocks in the Gibraltar Arc. *Arabian Journal of Geosciences*, 7(5), 1993–2005.
- Bache, F., Olivet, J.-L., Gorini, C., Aslanian, D., Labails, C., & Rabineau, M. (2010). Evolution of rifted continental margins: the case of the Gulf of Lions (Western Mediterranean Basin). *Earth and Planetary Science Letters*, 292, 345–356.
- Balanyá, J. C., García-Dueñas, V., Azañón, J. M., & Sánchez-Gómez, M. (1997). Alternating contractional and extensional events in the Alpujarride nappes of the Alboran domain (Betics, Gibraltar arc). *Tectonics*, 16(2), 226–238.
- Ballouard, C., Boulvais, P., Poujol, M., Gapais, D., Yamato, P., Tartèse, R., & Cuney, M. (2015). Tectonic record, magmatic history and hydrothermal alteration in the Hercynian Guérande leucogranite, Armorican Massif, France. *Lithos*, 220–223, 1–22.
- Barich, A., Acosta-Vigil, A., Garrido, C. J., Cesare, B., Tajcmanová, L., & Bartoli, O. (2014). Microstructures and petrology of melt inclusions in the anatectic sequence of Jubrique (Betic Cordillera, S Spain): implications for crustal anatexis. *Lithos*, 206–207, 303–320.
- Chalouan, A., Michard, A., El Kadiri, K., deFrizon Lamotte, D., Negro, F., Soto, J., & Saddiqi, O. (2008). The Rif belt. In A. Michard, O. Saddiqi, A. Chalouan & de Lamotte D. F. (Eds.), *Continental Evolution: the Geology of Morocco: Structure, Stratigraphy, and Tectonics of the Africa–Atlantic–Mediterranean Triple Junction* (pp. 203–302). Berlin: Springer.
- Cuevas, J., Esteban, J., & Tubía, J. (2006). Tectonic implications of the granite dike swarm in the Ronda Peridotites (Betic Cordilleras, southern Spain). *Journal of the Geological Society*, 163(4), 631–640.
- Duggen, S., Hoernle, K., van den Bogaard, P., & Harris, C. (2004). Magmatic evolution of the Alboran region: the role of subduction in forming the Western Mediterranean and causing the Messinian salinity crisis. *Earth and Planetary Science Letters*, 218(1–2), 91–108.

- Esteban, J.J., Sánchez-Rodríguez, L., Seward, D., Cuevas, J. and Tubía, J.M., (2004). The late thermal history of the Ronda area, southern Spain. *Tectonophysics*, 389(1–2), 81–92.
- Esteban, J. J., Cuevas, J., Tubía, J. M., Gil Iburguchi, J. I., & Seward, D. (2005). Metamorfismo, exhumación y termocronología de la Unidad de Yunquera (Alpujarrides occidentales, Cordilleras Béticas). *Revista de la Sociedad Geológica de España*, 18(1–2), 61–74.
- Esteban, J. J., Cuevas, J., Tubía, J. M., Liati, A., Seward, D., & Gebauer, D. (2007). Timing and origin of zircon-bearing chlorite schists in the Ronda peridotites (Betic Cordilleras, Southern Spain). *Lithos*, 99, 121–135.
- Esteban, J. J., Cuevas, J., Tubía, J., Sergeev, S., & Larionov, A. (2011). A revised Aquitanian age for the emplacement of the Ronda peridotites (Betic Cordilleras, southern Spain). *Geological Magazine*, 148(1), 183–187.
- Esteban, J. J., Tubía, J. M., Cuevas, J., Seward, D., Larionov, A., Sergeev, S., & Navarro-Vilá, F. (2013). Insights into extensional events in the Betic Cordilleras, southern Spain: new fission-track and U-Pb SHRIMP analyses. *Tectonophysics*, 603, 179–188.
- Frasca, G., Gueydan, F., & Brun, J.-P. (2015). Structural record of Lower Miocene westward Alboran Domain motion in the Western Betics (southern Spain). *Tectonophysics*, 657, 1–20.
- Frasca, G., Gueydan, F., Brun, J.-P., & Monié, P. (2016). Deformation mechanisms in a continental rift up to mantle exhumation. Field evidence from the western Betics, Spain. *Marine and Petroleum Geology*, 76, 1–19.
- Garrido, C. J., Gueydan, F., Booth-Rea, G., Précigout, J., Hidas, K., Padrón-Navarta, J. A., & Marchesi, C. (2011). Garnet lherzolite and garnet-spinel mylonite in the Ronda peridotite: vestiges of Oligocene backarc mantle lithospheric extension in the Western Mediterranean. *Geology*, 39(10), 927–930.
- Gueydan, F., Pitra, P., Afri, A., Poujol, M., Essaifi, A., & Paquette, J.-L. (2015). Oligo-Miocene thinning of the Beni Bousera peridotites and their Variscan crustal host rocks, Internal Rif, Morocco. *Tectonics*, 34, 1–25. doi:10.1002/2014TC003769
- Hidas, K., Booth-Rea, G., Garrido, C. J., Martínez-Martínez, J. M., Padrón-Navarta, J. A., Konc, Z., Giaconia, F., Frets, E., & Marchesi, C. (2013). Backarc basin inversion and subcontinental mantle emplacement in the crust: kilometre-scale folding and shearing at the base of the proto-Alborán lithospheric mantle (Betic Cordillera, southern Spain). *Journal of the Geological Society*, 170(1), 47–55.
- Hurford, A. J., Platt, J. P., & Carter, A. (1999). Fission-track analysis of samples from the Alboran Sea basement. In R. Zahn, M. C. Comas, & A. Klaus (Eds.), *Proceedings of the Ocean Drilling Program, Scientific Results*, 161(21), 295–300.
- Kelley, S. P., & Platt, J. P. (1999). Ar–Ar dating of biotite and muscovite from Alboran basement samples. In R. Zahn, M. C. Comas & A. Klaus (Eds.), *Proceedings of the Ocean Drilling Program, Scientific Results*, 161 (22), 301–305.
- Lundeen, M. (1978). Emplacement of the Ronda Peridotite, Sierra Bermeja, Spain. *Geological Society of America Bulletin*, 89, 172–180.
- Marchesi, C., Garrido, C. J., Bosch, D., Bodinier, J.-L., Hidas, K., Padrón-Navarta, J. A., & Gervilla, F. (2012). A Late Oligocene suprasubduction setting in the westernmost Mediterranean revealed by intrusive pyroxenite dikes in the Ronda peridotite (southern Spain). *The Journal of Geology*, 120(2), 237–247.
- Massonne, H.-J. (2014). Wealth of P–T–t information in medium-high grade metapelites: example from the Jubrique Unit of the Betic Cordillera, S Spain. *Lithos*, 208–209, 137–157.
- Mazzoli, S., & Martín-Algarra, A. (2011). Deformation partitioning during transpressional emplacement of a 'mantle extrusion wedge': the Ronda peridotites, Western Betic Cordillera, Spain. *Journal of the Geological Society of London*, 168, 373–382.
- Monié, P., Torres-Roldán, R., & García-Casco, A. (1994). Cooling and exhumation of the Western Betic Cordillera, $^{40}\text{Ar}/^{39}\text{Ar}$ thermochronological constraints on a collapsed terrane. *Tectonophysics*, 238(1–4), 353–379.
- Michard, A., Negro, F., Saddiqi, O., Bouybaouene, M.L., Chalouan, A., Montigny, R. and Goffé, B., (2006). Pressure-temperature-time constraints on the Maghrebide mountain building: evidence from the Rif-Betic transect (Morocco, Spain), Algerian correlations, and geodynamic implications. *C. R. Geoscience*, 338, 92–114.
- Negro, F., Beyssac, O., Goffé, B., Saddiqi, O., & Bouybaouéne, M. L. (2006). Thermal structure of the Alboran Domain in the Rif (northern Morocco) and the Western Betics (southern Spain). Constraints from Raman spectroscopy of carbonaceous material. *Journal of Metamorphic Geology*, 24(4), 309–327.
- Platt, J. P., Argles, T., Carter, A., Kelley, S., Whitehouse, M., & Lonergan, L. (2003). Exhumation of the Ronda peridotite and its crustal envelope: constraints from thermal modelling of a P–T–time array. *Journal of the Geological Society*, 160(5), 655–676.
- Platt, J. P., & Whitehouse, M. (1999). Early Miocene high-temperature metamorphism and rapid exhumation in the Betic Cordillera (Spain): evidence from U–Pb zircon ages. *Earth and Planetary Science Letters*, 171(4), 591–605.
- Platt, J. P., Whitehouse, M., Kelley, S., Carter, A., & Hollick, L. (2003). Simultaneous extensional exhumation across the Alboran Basin: implications for the causes of late orogenic extension. *Geology*, 31(3), 251–254.
- Précigout, J., Gueydan, F., Garrido, C. J., Cogné, N., & Booth-Rea, G. (2013). Deformation and exhumation of the Ronda Peridotite (Spain). *Tectonics*, 32(4), 1011–1025.
- Rossetti, F., Dini, A., Lucci, F., Bouybaouenne, M., & Faccenna, C. (2013). Early Miocene strike-slip tectonics and granite emplacement in the Alboran Domain (Rif chain, Morocco): significance for the geodynamic evolution of Western Mediterranean. *Tectonophysics*, 608, 774–791.
- Rossetti, F., Theye, T., Lucci, F., Bouybaouenne, M., Dini, A., Gerdes, A., Phillips, D., & Cozzupoli, D. (2010). Timing and modes of granite magmatism in the core of the Alboran Domain, Rif chain, northern Morocco: Implications for the alpine evolution of Western Mediterranean. *Tectonics*, 29, TC2017.
- Ruiz Cruz, M. D., & Sanz de Galdeano, C. (2014). Garnet variety and zircon ages in UHP meta-sedimentary rocks from the Jubrique Zone (Alpujarride complex, Betic Cordillera, Spain): evidence for a pre-alpine emplacement of the Ronda Peridotites. *International Geology Review*, 56(7), 845–868.
- Sánchez-Navas, A., García-Casco, A., & Martín-Algarra, A. (2014). Pre-Alpine discordant granitic dikes in the metamorphic core of the Betic Cordillera: tectonic implications. *Terra Nova*, 26(6), 477–486.
- Sánchez-Rodríguez, L., & Gebauer, D. (2000). Mesozoic formation of pyroxenites and gabbros in the Ronda area (southern Spain), followed by Early Miocene subduction metamorphism and emplacement into the middle crust: U–Pb sensitive high-resolution ion microprobe dating of zircon. *Tectonophysics*, 316(1–2), 19–44.
- Serrano, F., Guerra-Merchán, A., Kadiri, K. E., Sanz de Galdeano, C., López-Garrido, A. C., Martín-Martín, M., & Hlila, R. (2007). Tectono-sedimentary setting of the Oligocene– Early Miocene deposits on the Betic-Rifian Internal Zone (Spain and Morocco). *Geobios*, 40(2), 191–205.
- Sosson, M., Morrillon, A.-C., Bourgois, J., Féraud, G., Poupeau, G., & Saint-Marc, P. (1998). Late exhumation stages of the Alpujarride complex (western Betic Cordilleras, Spain): new thermochronological and structural data on Los Reales and Ojen nappes. *Tectonophysics*, 285(3–4), 253–273.
- Tubía, J., Cuevas, J., & Iburguchi, J. G. (1997). Sequential development of the metamorphic aureole beneath the Ronda Peridotites and its bearing on the tectonic evolution of the Betic Cordillera. *Tectonophysics*, 279(1), 227–252.

- Turcotte, D. L., & Schubert, G. (1982). *Geodynamics: Applications of Continuum Physics to Geological Problems* (pp. 1–450). New York, NY: John Wiley & Sons.
- Van der Wal, D. and Vissers, R.L.M., (1993). Uplift and emplacement of upper mantle rocks in the western Mediterranean. *Geology*, 21, 1119–1122.
- Van Hinsbergen, D. J. J., Vissers, R. L. M., & Spakman, W. (2014). Origin and consequences of Western Mediterranean subduction, rollback, and slab segmentation. *Tectonics*, 33(4), 393–419.
- Vitale, S., Zaghoul, M. N., Tramparulo, F. D., & Ouaragli, B. E. (2014). Deformation characterization of a regional thrust zone in the northern Rif (Chefchaouen, Morocco). *Journal of Geodynamics*, 77, 22–38.
- Whitehouse, M., & Platt, J. (2003). Dating high-grade metamorphism - constraints from rare-earth elements in zircon and garnet. *Contributions to Mineralogy and Petrology*, 145(1), 61–74.
- Wortel, M. J. R., & Spakman, W. (2000). Subduction and slab detachment in the Mediterranean-Carpathian region. *Science*, 209, 1910–1917.

SUPPORTING INFORMATION

Additional Supporting Information may be found online in the supporting information tab for this article.

How to cite this article: Frasca G, Gueydan F, Poujol M, et al. Fast switch from extensional exhumation to thrusting of the Ronda Peridotites (South Spain). *Terra Nova*. 2017;29:117–126. <https://doi.org/10.1111/ter.12255>